JOURNAL OF AIRCRAFT
Vol. 32, No. 3, May–June 1995

Nonlinear Aerodynamic Analysis of Grid Fin Configurations

John E. Burkhalter,* Roy J. Hartfield,† and Todd M. Leleux‡
Auburn University, Auburn, Alabama 36849

An aerodynamic analysis of generalized grid fin configurations has been completed for subsonic flow. Grid fins are lifting surface devices that may be used as control surfaces for general missile configurations. A preprocessor code has been developed that designs the grid fin from general geometric input. Designs that are not practical are rejected and graphical drawings of the configuration under consideration are displayed for review purposes. The theoretical analysis is fundamentally based on a vortex lattice overlay of the lifting elements that produces adequate modeling for small angles of attack. For higher angles of attack, empirical equations are used for the body and fin aerodynamic coefficients. Good agreement between experimental data and theoretical predictions are obtained for the grid fins considered up to angles of attack of about 45 deg. For other grid fin designs, the agreement between the theory and experimental results has not yet been determined.

Nomenclature

A_b = body cross-sectional area
A_p = fin or body planform area
C_{av} = axial force coefficient for the top and bottom fins, nos. 1 and 2
C_{ax} = fin axial force coefficient
$C_{ax\,b}$ = body axial force coefficient
C_{dbfc} = friction drag coefficient for the body
C_{dbp} = body base pressure drag coefficient
C_{dc} = body crossflow drag coefficient
C_{dow} = fin viscous friction drag coefficient
C_{dp} = fin pressure drag coefficient
C_{dxp} = fin interference drag coefficient
C_{mhg} = fin hinge moment coefficient about the fin hinge line
C_{mle} = fin hinge moment coefficient about the fin leading edge
C_{mmcb} = moment coefficient produced by the body about the moment center
C_{mmcf} = moment coefficient produced by the fin about the moment center
C_{mv} = pitching moment coefficient for the top and bottom fins, nos. 1 and 2
C_{Nb} = normal force coefficient for the body
C_{NJ} = body normal force coefficient at an angle of attack of $\pi/8$, Jorgensen's theory
$C_{N\mathrm{wash}}$ = normal force coefficient due to body upwash
C_{N45} = fin normal force coefficient at an angle of attack of 45 deg
$C_{N\alpha}$ = normal force coefficient slope, $dC_N/d\alpha$
$C_{N\alpha\text{-off}}$ = normal force coefficient slope for body upwash turned "off"
$C_{N\alpha\text{-on}}$ = normal force coefficient slope for body upwash turned "on"
C_{nf} = fin normal force coefficient as computed from vortex lattice theory
C_{nff} = fin normal force coefficient, total
C_{nv} = normal force coefficient for the top and bottom fins, nos. 1 and 3
C_{rcbm} = fin root chord bending moment coefficient
c_r = fin chord length
fr = fineness ratio
L_b = total length of the body
L_{ref} = reference length for the configuration
M = Mach number
np = number of fin element intersection points
q_∞ = freestream dynamic pressure
R_b = radius of the body, max
Re = Reynolds number based on body length
R_t = radius of the body at the aft end
S_{ref} = reference area for the configuration
$S_{\mathrm{wet}\,b}$ = body wetted area
$S_{\mathrm{wet}\,w}$ = fin wetted area
t = thickness of an element of a grid fin
V = body volume
X_{cb} = axial distance from the nose to the body neutral point
X_{hing} = axial distance from the nose to the fin hinge line
X_{mc} = axial distance from the nose to the moment center
α = angle of attack
δ = fin incidence angle
η = crossflow drag proportionality factor, ratio of crossflow drag for a finite length cylinder to that for an infinite length cylinder

Received Feb. 23, 1994; revision received July 21, 1994; accepted for publication Sept. 15, 1994.

*Associate Professor, Aerospace Engineering Department. Associate Fellow AIAA.
†Assistant Professor, Aerospace Engineering Department. Member AIAA.
‡Graduate Research Assistant, Aerospace Engineering Department. Member AIAA.

Introduction

EVEN though grid fins have been in use for several years as lifting surface control devices on certain missile configurations,[1] they are still considered an unconventional lifting surface. Theoretical developments have lagged in the usage of these devices and, to date, much of the internal flowfield associated with the grid elements is still unknown. Figure 1 provides a three-dimensional view of a typical grid fin application and pictures the grid elements lattice network inside a rigid outer boundary. The attractiveness of a grid fin over a conventional fin is based on the fact that grid fins do not "stall" in the conventional sense, but continue to produce lift even at very high angles of attack, and the fact that the hinge moments (actuator requirements) are extremely low because of the small chord length. The fundamental problem, in the present study, was to develop the theoretical methodology to predict the aerodynamic forces and moments produced by the grid fin lifting surface as it is attached to a missile body as shown in Fig. 1.

For subsonic flow, efforts to model and understand the grid fin have centered around a vortex lattice formulation[1,2] and many published techniques have utilized experimental

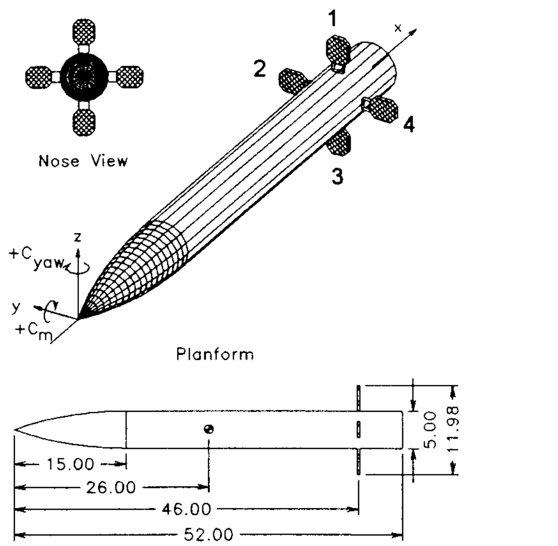

Fig. 1 Configuration for a cruciform grid fin set with a supporting missile body.

data[3–7] extensively. In most of these studies, little basic theoretical work was done and an understanding of the problem has relied on an analysis of experimental data. The lattice formulation as presented in Ref. 1 does not offer a concise treatment of the problem, and the solution as presented in Ref. 2 is valid only for small angles of attack. However, the vortex lattice methodology is clearly established and is consequently used in the present work.

Modeling the grid fin with a purely theoretical formulation requires techniques that encompass multiple lifting surfaces oriented at angles other than the traditional "wing" plane. For this reason, and perhaps others, little work from a purely theoretical standpoint has been completed. However, the nature of the grid fin geometry lends itself to a vortex lattice formulation. Consequently, for the present study a vortex lattice solution has been used for basic theoretical modeling at low angles of attack, and empirical formulas based on existing wind-tunnel data have been used for angles up to 60 deg. Wind-tunnel test results from Refs. 6–8 have been used extensively for the higher angle-of-attack range in developing equations for grid fin aerodynamic coefficients.

The present work has encompassed both the development of a preprocessing code for designing geometrically realistic grid fins that can be theoretically modeled with a vortex lattice formulation and the theoretical and empirical modeling of aerodynamic coefficients for grid fins up to 60-deg angle of attack. Also included in this analysis are the computations for the fin-body loads, the fin-body carryover loads, and the upwash generated by the body on the grid fin.

The analyses presented herein are applied to both the grid fin and the grid fin supporting structure, which, in this case, is a missile body. A schematic of the generic fin-body system modeled for this work is shown in Fig. 1. In some cases, the grid fin structures will be curved so that the grid structure can be folded against the missile body when in a prelaunch configuration or when stored in a carriage configuration. However, for the present analysis, only the aerodynamics for flat grid fin geometries as shown in Fig. 1 are considered. From experimental data,[5] however, it has been shown that a small amount of curvature does not substantially alter the aerodynamic performance of the grid fin structure.

Theoretical Analysis

The theoretical development for placing a system of vortices on a generic grid fin closely follows that of Ref. 2. Each grid cell is made up of a four-sided parallelogram and vortices are placed on each of these sides. An element is defined to be one of the sides of the parallelogram on which the bound portion of vortices are placed. An element is divided into a rectangular array of subelements (lattice network) and on each subelement a single bound vortex is placed along the quarter-chord of the subelement. For the grid fin as shown in Fig. 2 (first designed in Ref. 2) the number of elements required to model the fin, including the support brackets, was 89. That is, there are 89 panels connected between 48 total intersection points. Usually, a large number of vortices placed on each element is not required for good accuracy, and the use of a "single" vortex on each element will accurately predict grid fin loading for most cases.

Grid Fin Design

In designing a grid fin for some specific missile application, the goal is no different from a planar fin design. For the present case, a generic design was considered since the methodology for analytical analysis was the overriding constraint. The geometric constraints, which may not be obvious at first, dictate the final grid density and subsequently the final lift, drag, and pitching moment produced by the fin. The number of elements and restrictions on how they are connected, especially at the corners, dictate the design. In the present design process, connecting elements at the element midpoint or at some location other than the end of the element, was not allowed. However, one has considerable flexibility in designing a fin and most fins of practical interest can be designed by the present procedure. Only fins that are symmetric with respect to a horizontal axis and only cells that are parallelogram in shape were considered. From Fig. 2 the variables that may be selected by the designer are 1) the overall fin span, 2) the distance the fin is offset from the body centerline, 3) the overall fin height, 4) the number of cells in the vertical (z) direction and the number of cells in the horizontal (y) direction, and 5) the type corner desired on the fin.

The logic for the design of a grid fin is illustrated by the sketch in Fig. 2. The "grid" points for the fin are defined as any point where two lines intersect. For the structure that supports the fin on the missile body, the grid points must be defined directly (manually), whereas the remaining grid points are defined automatically using a marching scheme in the vertical and horizontal direction. A boundary must be established in the vertical and horizontal direction and as many points as possible are defined within this boundary. In the design algorithm developed for the present analysis, the in-

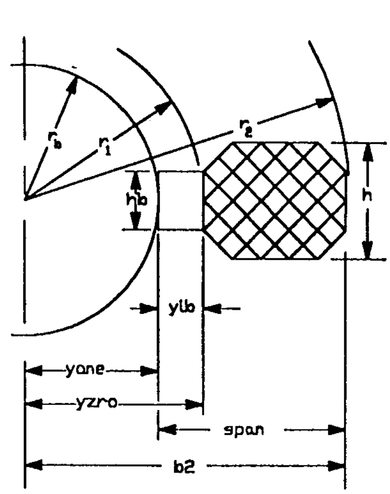

r_b = 2.5	r_1 = 3.327
r_2 = 6.02	hb = 1.07
h = 2.14	ylb = .828
yone = 2.5	yzro = 3.328
span = 3.49	b2 = 5.99

Fig. 2 Schematic of a grid fin layout on a missile body.

tersection points are first established and then logic to connect the points is initiated. However, even though an array of points may be defined within or on the boundary of the grid fin, they may or may not be "connected" as part of the final design. Constraints were established from the overall geometry that dictated which points would finally form an element in the grid fin. The constraints established in the design algorithm consisted of boundary limits that eliminated unwanted points. In the design process, the following constraint limitations were established:

1) No points were placed inside the radius designated as r1, except those constituting the base support structure.

2) No points were placed outside the radius designated as r2.

3) No points were placed inside the lateral dimension designated as yzro, except those constituting the base support structure.

4) The shape of the fin at the base was determined by the value of the variable *ibase*, which determines if the base is to be square or is to be truncated to cover one or two cells.

5) The shape of the fin at the tip is determined by the value of the variable *itip* and by the number of delta y increments. In the design algorithm, if *itip* has been set to 1 or 2, the fin is chamfered at the corners. The amount of chamfer is established purely by number of delta y increments and is not part of the design selection process. However, a corner cell will not be cut in such a way to form an intersection point that does not conform to the remaining restrictions established in the program. If *itip* is input as 0.0, the corner of the fin will be 90 deg (rectangular) and no chamfer is made.

6) In the y direction, half-delta y increments were allowed, whereas in the vertical direction, only whole increments were allowed. The reason for this restriction is to insure that the fin has symmetry about the horizontal (y) axis.

After all correct coordinate locations for all points are defined, the logic to "connect" the points was initiated and the "elements" that make up the grid fin structure were established.

Vortex Lattice Solution

A vortex lattice solution was used to model the grid fin lattice network as well as the grid fin support structure. That is, vortices were placed on both the elements that make up the grid lattice and the elements that make up the support structure. The entire system of elements, therefore, constituted a fin design and determined the loading carried by the "grid fin." Apart from the geometric considerations, the aerodynamic fin-body carryover loads and the loading created by the missile body upwash were also included in the analysis.

For body upwash considerations, the axisymmetric body was modeled as an infinite cylinder composed of an infinite line doublet. Efforts to model the body with point sources/sinks and doublets were completed in previous studies[2,3] and were successful in computing the additional loads due to upwash. However, a comparison of the source/sink-doublet solution and the infinite line doublet solution revealed that little difference existed between the two approaches, with the exception that, for the source/sink-doublet solution, the computer run time increased. Consequently, the source/sink-doublet solution was abandoned and an infinite line doublet was employed in all subsequent analyses.

The wing carryover loads were modeled by imaging the grid fin "wing" inside the body. The procedure is relatively simple and realistic carryover loads were obtained. It should be pointed out that because of small semispans for general grid fin applications, modeling the wing carryover loads is essential. For the designs considered in this report, these loads constituted about one-third of the total.

Normal Force

Since the vortex lattice formulation is a potential flow, inviscid solution, it is valid only in the linear angle of attack range that in this case is about 5–8 deg. Obviously, this is inadequate for general grid fin applications; consequently, existing experimental data was used to extend the range beyond the vortex lattice limit up to (and beyond) 45 deg angle of attack. It is strongly stressed that this extension to higher angles has not been tested or applied to generic designs and it is not known, at this point, how well the equations apply to general configurations. Nevertheless the methods that were utilized were based on logical assumptions and basic aerodynamic principles. Therefore, it is believed that the general principles apply to other configurations, and the resulting empirical equations provide a good design methodology for general grid fin configurations.

The key to an empirical extension to higher angles of attack is strongly dependent on an accurate computation of the fin normal force. The form of the equation is based on the observation that grid fins do not stall in the normal aerodynamic sense, but continue to produce lift even at large angles of attack. The lift production does, however, peak. Therefore, the required equation must define a curve that has the traditional linear slope at $\alpha = 0$ and demonstrates a peak value at a large angle of attack. For the present case, experimental data[5–7] indicates that the grid fin maximum normal forces peak at about 45 deg, and thus, this value was chosen as the angle of attack at which maximum lift occurs.

The grid fin experiences an additional aerodynamic force associated with body upwash effects. If the aerodynamics of the grid fin and the body upwash were linear over the range of angles of attack of interest, then the upwash terms could be included in general expressions for the normal force coefficient. However, since these terms are nonlinear and because the body can be at one angle of attack α, and the fin may be at a different absolute angle of attack $\alpha + \delta$, it is necessary to separate the fin alone terms from the body upwash terms. This may be illustrated by considering the following: at an angle of attack of zero and a fin incidence δ, the fin will produce lift indicative of the angle δ, but will be void of the body upwash contribution. At a fin-body angle of attack, α, which is the same value as in the previous case but with no fin incidence, the fin produces a different normal force that now includes the body upwash contribution. Consequently, it was assumed that the normal force for the fin could be divided into two distinct terms. The first term, which does not include any body upwash effects, is due to the fin absolute angle of attack $\alpha + \delta$, and the second is due to the body induced upwash dependent only on the body α. It is further required that the first term have a linear slope at $\alpha + \delta = 0$, and the second term must describe the loading due to the body upwash. From experimental data, it has been determined that an appropriate form of the parametric equation for the normal force coefficient for the horizontal fins is

$$C_N = \frac{C_{N\alpha}(\alpha + \delta)}{1.0 + K_1(\alpha + \delta)^2} + C_{N_{\text{wash}}} \tag{1}$$

where α is the body angle of attack, δ is the fin incidence angle, $C_{N\alpha}$ is the fin lift curve slope at $\alpha = 0$, and the constant K_1 still has to be determined. The lift curve slope $C_{N\alpha}$ may be obtained from the vortex lattice solution as previously discussed, however, the problem of finding the constant in the equation and the fin normal force due to upwash is not straightforward.

In order to find the fin normal force due to body upwash, consider the special case of a fin configuration attached to a body with the body at an angle of attack of 0.0 and the fin at some small deflection angle δ, e.g., 5 deg. In this case, the body upwash is zero, therefore, the second term in Eq. (1) does not exist and the fin normal force coefficient may be written as

$$C_N = \frac{C_{N\alpha}\alpha_A}{1.0 + K_1\alpha_A^2} \tag{2}$$

where, in general, $\alpha_A = \alpha + \delta$, the absolute angle of attack of the fin. The vortex lattice solution would certainly apply for this case since it clearly falls within the linear range. Now consider a second case, with the body/fin at the same absolute angle of attack as before, but in this case let δ be zero and α = 5 deg. At this small angle of attack, the vortex lattice solution still applies and the normal force coefficient may be found that includes the body upwash effects as generated by an infinite line doublet along the centerline of the body.

The difference between these two solutions for the normal force must be due to the body upwash. Even though this "differencing" approach would be unnecessary for small angles of attack, it is necessary for angles above the linear range. For the general case of a body at angle of attack and fin at some incidence angle, outside the linear range, it is then assumed that the body upwash contribution to fin normal force does not change with fin incidence, but is dependent only on the body α.

In order to evaluate the constant K_1 in Eq. (1), the following observations were made from experimental data.

1) The fin normal force appears to reach a maximum at an absolute angle of attack of about 45 deg.

2) At this angle, the fin alone normal force (exclusive of any body upwash effects) may be determined by assuming that the fin frontal area appears as a near solid block and the normal force can be expressed as

$$N_{45} = (fb)q_\infty \sin(45)(2) \tag{3}$$

Here (fb) is the "flow blockage area" and the (2) is for two fins (right and left). In the above equation, it has also been assumed that the force coefficient is 1.0, which is quite reasonable for a "near" solid block. In coefficient form, Eq. (3) becomes

$$C_{N45} = \frac{(fb)\sqrt{(2)}}{S_{\text{ref}}} \tag{4}$$

If Eq. (4) is substituted into Eq. (2), then K may be determined as

$$K = 16.0[C_{N\alpha}(\pi/4) - C_{N45}]/(\pi^2 C_{N45}) \tag{5}$$

Now if the vortex lattice solution is obtained, turning the body upwash on, then the constant K in Eq. (2) may be found using Eq. (5) with the resulting normal force coefficient designated as $C_{N\text{-on}}$. If the process is repeated with the upwash turned off, then the normal force coefficient is designated as $C_{N\text{-off}}$. The difference between these two cases, as previously discussed, is the fin normal force due to the upwash created by the body on the fins and must be equal to the second term in Eq. (1). That is

$$\text{dif} = \left(\frac{C_{N\alpha\text{-on}}\alpha_A}{1.0 + K_{\text{on}}\alpha_A^2} - \frac{C_{N\alpha\text{-off}}\alpha_A}{1.0 + K_{\text{off}}\alpha_A^2}\right) = C_{N_{\text{wash}}} \tag{6}$$

From experimental data, this method of determining the body upwash contribution to the fin normal force in the nonlinear alpha range appears to be adequate at least for body angles of attack up to 20 deg, but for body angles of attack above 20 deg, the method is unproven.

In summary, the computational procedure for determining the fin normal force is as follows:

1) Given, a body α, a δ, and the geometry of the fin to compute fb. The absolute angle of attack for the fin is $\alpha_A = \alpha + \delta$.

2) Initially set the "angle of attack" to 5.0 deg and use the vortex lattice code alone to determine $C_{N\alpha\text{-on}}$ for the case where the body is present.

3) Repeat the process, but delete the body from the computations and determine a value of $C_{N\alpha\text{-off}}$.

4) Determine C_{N45} from Eq. (4).

5) Compute K_{on} from Eq. (5), using the value of $C_{N\alpha\text{-on}}$ found in 1 above.

6) Compute K_{off} from Eq. (5), using the value of $C_{N\alpha\text{-off}}$ found in 2 above.

7) At each angle of attack and fin deflection angle, determine the upwash coefficient from Eq. (6). Find the fin normal force coefficient from Eq. (1) in which K_1 is the same as K_{off}.

Fin Moments

The horizontal fins produce moments about the hinge line that are very small and are computed partially from the vortex lattice solution and partially from empirical factors. The moments about the fin leading edge are computed by integrating sectional properties along the span for an initial angle of attack of 5.0 deg. These moments about the leading edge are then transferred to the hinge line for evaluation of the fin hinge moments. At higher angles of attack, the value of the moment about the leading edge is approximated by multiplying the value at 5 deg by the ratio of the respective normal forces. Consequently, the hinge moments for the fin become

$$C_{mhg} = C_{mle}(C_{nff}/C_{nf}) + C_{nff}[C_r/(2.0L_{\text{ref}})] \tag{7}$$

where C_{nf} is the vortex lattice normal force coefficient at 5 deg and C_{nff} is the actual nonlinear fin normal force coefficient as computed from Eq. (1). Equation (7) may be derived by assuming that the c.p. on the fin chord does not change at higher angles of attack, and by observing that the fin chord is centered over the hinge line. Actually, the c.p. does shift aft at higher angles of attack, but the chord is very small and the chordwise shift is small. The root chord bending moments are computed in a similar fashion as

$$C_{rcbm} = C_{rcbm_{(5°)}}(C_{nff}/C_{nf}) \tag{8}$$

and finally, the moment about the configuration moment center is

$$C_{mmcf} = C_{mhg} - C_{nff}[(X_{\text{hing}} - X_{mc})/L_{\text{ref}}] \tag{9}$$

Axial Force

The axial force on the fin (drag at $\alpha = 0.0$) is assumed to be composed of skin friction, pressure drag, and an interference drag due to fin element intersections. For the skin friction drag, the fin wetted area is computed and converted to an equivalent "flat plate" with an assumed laminar and/or turbulent boundary layer. The skin friction coefficient, as a function of Reynolds number, is determined and finally a friction axial force coefficient is computed as C_{dow}. These computations for viscous axial force follow closely those in Ref. 8. It is assumed that the pressure drag takes the form of

$$\text{pressure drag}_{\alpha=0} = q_\infty(\text{frontal area}) \tag{10}$$

In coefficient form, this results in

$$C_{dp} = (S_{\text{wetw}}t)/(S_{\text{ref}}c_r) \tag{11}$$

Finally, the element intersections create a drag that is empirically determined from experimental data[5-7] as

$$C_{dxp} = 2.0 \times 0.000547 \times (np + 2) \tag{12}$$

where $(np + 2)$ is the total number of grid intersection points including points on the base support structure. The axial force coefficient is then the sum of these three components:

$$C_{ax} = C_{dow} + C_{dxp} + C_{dp} \tag{13}$$

From experimental grid fin data, the fin axial force coefficient changes very little over a large range of angles of attack,[5,6] consequently, it was assumed that the axial force is independent of angle of attack and is therefore constant at the value determined in Eq. (13).

Body Aerodynamic Coefficients

The body alone aerodynamic coefficients are based on a combination of Jorgensen's theory[9] and a modified form of slender body theory. Jorgensen's theory has been shown to yield good agreement with experimental results, at least for angles of attack between 30–60 deg. For lower angles of attack between 0–20 deg, the theory does not agree quite as well; consequently, a modified form of slender body theory was used.

Body Normal Force

In order to utilize this modified slender body theory in conjunction with Jorgensen's theory, it was required that the normal force coefficient from each theory coincide at an angle of attack of about 20 deg (specifically $\pi/8$). In the present method for body angles of attack below 20 deg, it is assumed that the modified slender body normal force coefficient may be written as

$$C_{Nb} = 2K_b\alpha/[K_b - \sin(2\alpha)] \tag{14}$$

where the constant K_b is determined by forcing agreement with Jorgensen's theory at an angle of attack of $\pi/8$. From this approach K_b is determined to be

$$K_b = C_{NJ}/\{\sqrt{2}[C_{NJ} - (\pi/4)]\} \tag{15}$$

For body angles of attack above 20 deg, the normal force coefficient equation of Jorgensen is used and is written as

$$C_{Nb} = (A_b/S_{\text{ref}})\sin(2\alpha)\cos(\alpha/2) + \eta C_{cd}(A_p/S_{\text{ref}})\sin^2\alpha \tag{16}$$

Body Pitching Moment

Jorgensen's method may also be used to compute the body alone pitching moment. For angles of attack between 20–60 deg, the equation for the body pitching moment is

$$C_{mmcb} = \left[\frac{V - A_b(L_b - X_{mc})}{S_{\text{ref}}L_{\text{ref}}}\right]\sin(2\alpha)\cos\left(\frac{\alpha}{2}\right) + \eta C_{dc}\frac{A_p}{S_{\text{ref}}}\left(\frac{X_{mc} - X_{cb}}{L_{\text{ref}}}\right)\sin^2\alpha \tag{17}$$

However, the pitching moment predicted by Jorgensen's method does not agree with experimental data as well as desired, especially at angles of attack below 20 deg. Consequently, extensive sets of experimental data[10] from several body alone wind-tunnel tests were used to develop an equation that identifies the body alone c.p. from which the body pitching moment could be determined. The empirical equation for the body alone neutral point resulting from this study was determined to be

$$X_{cb} = (L_b/2)\{1 - 1/[2 + (L_b/R_b)\alpha^2]\} \tag{18}$$

so that the pitching moment coefficient for the body about the moment center is

$$C_{mmcb} = C_{Nb}[(X_{mc} - X_{cb})/L_{\text{ref}}] \tag{19}$$

Equation (19) is used for determining the body pitching moment for angles of attack below 20 deg, and Eq. (17) may be used for angles above this value, even though in the present study the body angle of attack range is limited to 20 deg.

Body Axial Force

The axial force for the body at small angles of attack is assumed to be composed of the skin friction contribution and the body base drag contribution. The equations that are used to compute these coefficients are taken from Ref. 8 and are presented here in summary form. The body fineness ratio and approximate body wetted area are

$$fr = L_b/(2R_b), \qquad S_{\text{wet}\,b} = 2\pi R_b L_b(0.7) \tag{20}$$

The friction coefficient for the body is

$$C_{dbfc} = C_{fb}[1 + (60/fr^3) + 0.0025fr]S_{\text{wet}\,b}/S_{\text{ref}} \tag{21}$$

where the Mach number and Reynolds number dependency from Ref. 8 has been curve-fitted as

$$C_{fb} = \left\{\frac{4.2109}{[\ell_n(Re)]^{2.642}}\right\}(1.10827 - 0.0852M^{1.5}) \tag{22}$$

The base pressure drag coefficient is

$$C_{dbp} = (0.029/\sqrt{C_{dbfc}})(R_t/R_b)^3 \tag{23}$$

where R_t is the radius of the body at the end of the boat-tail. From an analysis of experimental body alone wind-tunnel data, it is assumed that the body axial force remains constant over the angle-of-attack range and is designated as C_{axb} so that

$$C_{\text{ax}\,b} = C_{dbfc} + C_{dbp} \tag{24}$$

It will be shown later that this assumption of constant body axial force is well-justified.

Results and Comparison with Experimental Data

Using the model shown in Figs. 1 and 2, the theoretical analysis was compared with data from Refs. 4–7. The entire test model consisted of four fins that were mounted horizontally and vertically. Fins number 2 and 4 are mounted in the horizontal as shown in Fig. 1, and fins 1 and 3 are mounted in the vertical on top and bottom of the missile airframe. Data were collected for configurations that included 1) the body alone, 2) two horizontal fins, and 3) the entire four-fin arrangement. For some of the tests, fins two and four were mounted on individual fin balances and were rotatable to discrete incidence angles, whereas fins one and three were fixed and rigidly attached to the body. Comparisons between the experimental data and the theoretical computations were made for several configuration combinations. In all experimental test data, the Mach number was maintained at $M = 0.5$, and the Reynolds number, based on the body diameter, was held constant at 2.27×10^7. For these tests, the standard body-fixed sign convention was used as shown in Fig. 1. All linear dimensions were nondimensionalized by the span of a single grid fin (see Fig. 2), which is analogous to the wing semispan on normal wing body combinations. The reference length was the maximum body diameter (5.0 in.) and the reference area was the maximum body cross-sectional area.

Body Alone

Figures 3 and 4 are plots of the body alone normal force, pitching moment, and axial force coefficients. Using the extensions supplied by Jorgensen's theory, the equations presented in the theoretical analysis are applicable for angles up through 60-deg total angle of attack, however, present experimental data does not extend beyond 20 deg and agreement for the present body/grid fin combination at higher angles is not known. Agreement up to 20-deg angle of attack is acceptable for this case for normal force and pitching moment,

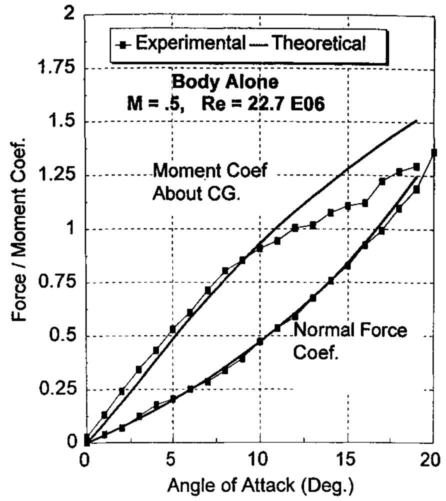

Fig. 3 Body alone normal force and pitching moment coefficient vs angle of attack.

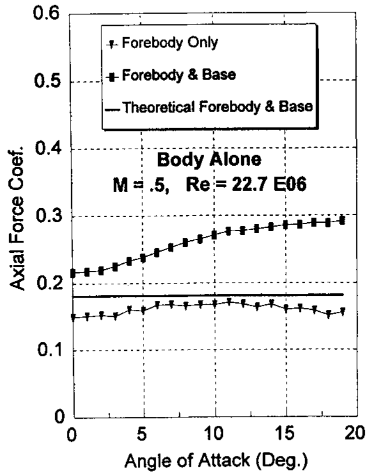

Fig. 4 Body alone axial force coefficient vs angle of attack.

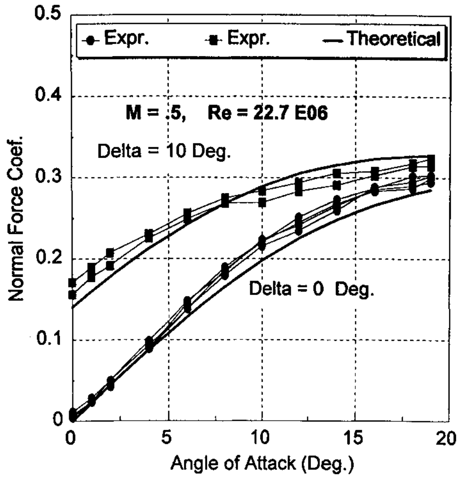

Fig. 5 Fin alone normal force coefficient for fin deflections of 0 and 10 deg vs angle of attack.

but the predicted axial force is low as shown in Fig. 4. It is believed that the major error in the axial force coefficient is in the base drag approximations and additional analyses are needed to correct this deficiency.

Fin Alone

Figures 5 and 6 are plots of fin no. 2 normal force coefficients showing a comparison of the theory with experimental

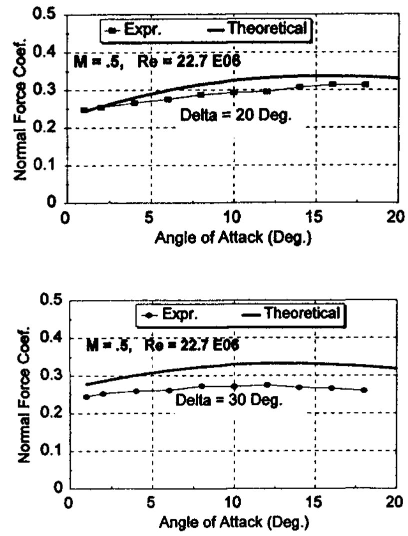

Fig. 6 Fin alone normal force coefficient for fin deflections of 20 and 30 deg vs angle of attack.

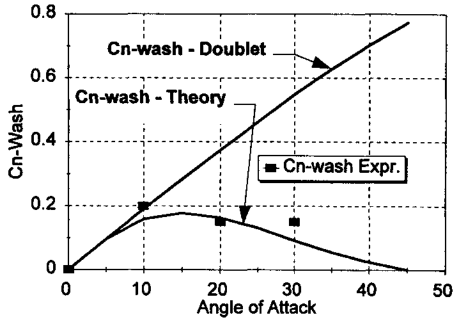

Fig. 7 Body upwash normal force coefficient vs angle of attack.

data at four different incidence angles. These figures were generated from an analysis of a single fin alone and do not include the wing-body carryover loads. The several lines of experimental data in these figures resulted from extracting fin no. 2 normal force coefficients from several sets of experimental data. Some of the data were obtained directly from "fin balances" and some were extracted from the main "body" balance. Considering the high angles involved in this case, the agreement is quite good. It is apparent from Fig. 6 that the fins do not actually stall in the classical aerodynamic sense. Somewhere between a fin total angle of attack of 30–50 deg, the normal force peaks, but there is no dropoff, as in a stall, even at 50 deg. By comparing these data with two-fin data to be presented later, it was determined that for the grid fin, a significant part of the load can be carried by the body as a wing carryover load.

Fin Normal Force Due to Body Upwash

It was assumed that the fin normal force could be separated into a nonbody-upwash term and a body upwash contribution as presented in Eq. (1). In order to validate this assumption and associated implications at a body angle of attack at 45 deg, computations for the theoretical upwash loading were isolated for the configuration involved in this study and the results are presented in Fig. 7. The "linear" result from the infinite line doublet is shown along with the nonlinear results from Eq. (6). A few data points could be extracted from the experimental data, and these are shown as rectangular symbols in Fig. 7. Clearly, the line doublet solution is not valid for angles greater than about 10 deg, and the present nonlinear results, from Eq. (6), do indeed agree with the experimental data. The experimental data point shown at 30 deg was obtained by extrapolating the $C_N - \alpha$ curve of Fig. 8 up to 30-deg angle of attack, and consequently, its accuracy is suspect. Clearly, the results agree quite well with the sparse experimental data, at least up to about 20 deg, but extrapolation beyond this range requires further analysis.

Fin Pair Loading with Body Upwash and Wing-Body Carryover Loads

Figure 8 is a comparison of the normal force, axial force, and pitching moment for a two-fin combination, which includes the wing-body carryover loads. Experimental data for these plots were obtained by isolating the normal force, pitching moment, and axial force for the top and bottom fins, fins one and three, and subtracting these forces and moments from the four-fin data. Fins one and three are "rigidly" attached to the body and develop less lift and pitching moment than fins two and four, especially at higher angles of attack.

Figure 9 is a plot of normal force, pitching moment, and axial force for the top and bottom fins, one and three. These data are somewhat irregular and were "smoothed" by curve fits over the range 0–20 deg as

$$C_{nv} = 0.0564 - 1.8515(\alpha - 0.174533)^2$$
$$C_{mv} = -0.300 + 9.8484(\alpha - 0.174533)^2 \qquad (25)$$
$$C_{av} = 0.087$$

Using the above equations to subtract the vertical fin forces and moments, the data for fins two and four were obtained and plotted in Fig. 8 for the zero incidence case. Agreement is good and Eq. (1) seems to provide the correct trends as well as the correct magnitude for the fin loads.

Figures 10–12 are similar comparison plots for fin incidence angles of 10, 20, and 30 deg, respectively. It is clear that for most of these cases, the agreement is good. The good agreement between the data and the theoretical modeling appears to break down at high incidence angles. However, it is clear that grid fins do not stall in the classical sense, but simply

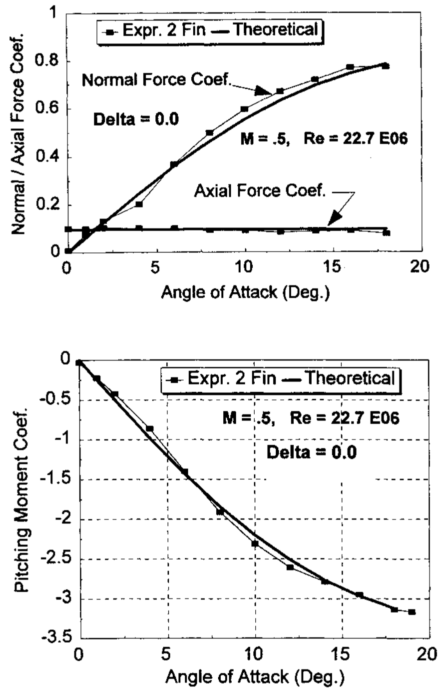

Fig. 8 Normal force, axial force and pitching moment coefficient for a fin deflection of zero deg vs angle of attack.

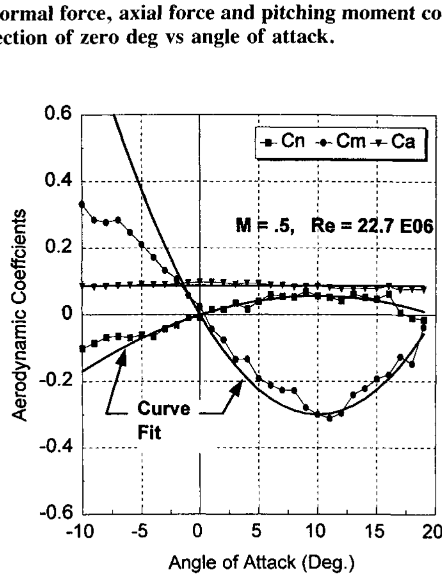

Fig. 9 Normal force, axial force, and pitching moment coefficient for vertical fins one and three vs angle of attack.

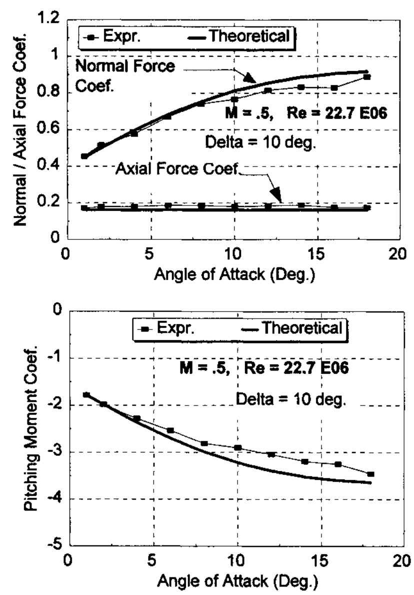

Fig. 10 Normal force, axial force, and pitching moment coefficient for a fin deflection of 10 deg vs angle of attack.

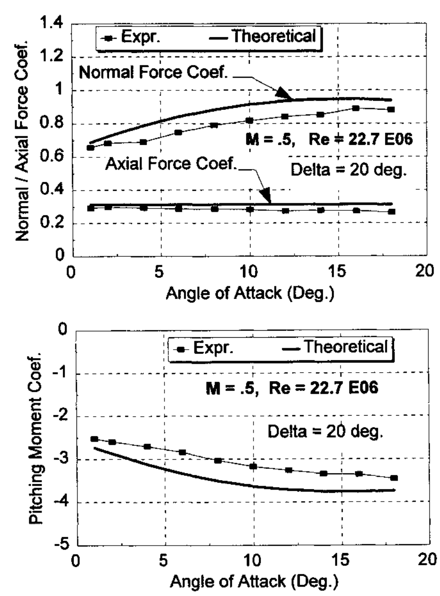

Fig. 11 Normal force, axial force, and pitching moment coefficient for a fin deflection of 20 deg vs angle of attack.

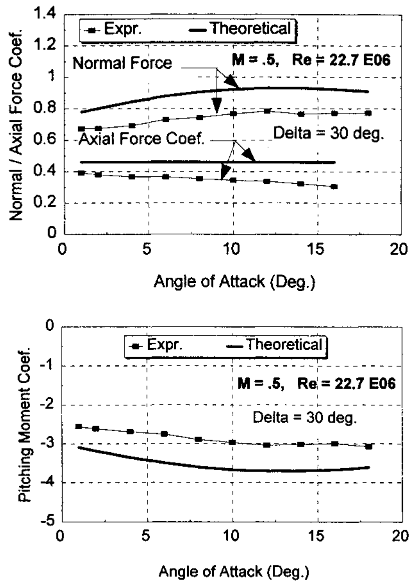

Fig. 12 Normal force, axial force, and pitching moment coefficient for a fin deflection of 30 deg vs angle of attack.

reach maximum (or minimum) values near the 45-deg total angle point. Even at 50 deg, there is no sharp drop in normal force nor any significant increase in pitching moment. Considering the high angles involved, the agreement is considered to be quite good.

For the cases where there are differences between the normal force coefficients, it appears that the initial assumptions are not quite valid and the upwash created by the body on the fin is not the same for differing fin deflection angles. However, given the large fin angles (up to a total of 50 deg for the 30-deg incidence case), the agreement between the experimental data and the theory is remarkable. It also seems that at high incidence angles, the assumption of constant axial force coefficient over the range of angles of attack is a valid assumption, but the methods used to compute the magnitude of the fin axial forces are somewhat in error. Further work should be done in this area to more accurately model the magnitude of the fin axial forces.

Experimental Accuracy

The balances used in the experimental wind-tunnel test included two fin balances attached to fins two and four, and a main balance with its electrical center at the moment center of the model (see Fig. 1). The quoted accuracy of the fin balances is 2.5% of the rated loads, which, in this case, results in an accuracy of ±5 lb for the normal force and ±5 in.-lb for the pitching moment. The main balance is quoted to be 0.25% of the rated loads or ±7 lb for the normal force, ±11 in.-lb for the pitching moment, and ±1 lb for the axial force. Even though the balance accuracy is quoted to have large uncertainties, the repeatability proved to be much better. In each case, the repeatability for each balance was quoted to be within 0.1% of rated loads.

Conclusions

As a result of the mathematical modeling and the analysis of the available experimental data, the following conclusions are made.

1) The algorithm for designing grid fins has proven to be satisfactory and implementation of the computer code provides the designer with a useful tool that eliminates considerable tedious work.

2) The theoretical methods developed for modeling the aerodynamics of grid fins appear to be adequate for design purposes. The empirical equations provide good agreement with experimental data over a wide range of angles of attack validating, to some extent, the assumptions made at the outset.

3) Although the agreement with experimental data for fins two and four appears to be very good up to about 50 deg, extension beyond this range has not been verified.

4) Modeling of the body forces and moments is adequate up to about 20 deg, but, for the present configuration, has not been validated for higher angles using Jorgensen's method.

References

[1]Belotserkovskiy, S. M., Odnovol, L. A., Safin, Yu. Z., Tyulenev, A. N., Frolov, V. P., and Shitov, V. A., "Wings with Internal Framework," Machine Translation, Foreign Technology Div., FTD-ID(RS)T-1289-86, Feb. 1987.

[2]Brooks, R. A., and Burkhalter, J. E., "Experimental and Analytical Analysis of Grid Fin Configurations," *Journal of Aircraft*, Vol. 26, No. 9, 1989, pp. 885–887.

[3]Burkhalter, J. E., and Brooks, R. A., "An Aerodynamic Analysis and Wind Tunnel Test of Several Grid Fin Configurations," Final Rept., U.S. Army Missile Command Contract DAAH01-85-D-A009-5, Sept. 1986.

[4]Washington, W. D., and Miller, M. S., "Grid Fins—A New Concept for Missile Stability and Control," AIAA Paper 93-0035, Jan. 1993.

[5]Washington, W. D., Booth, P. F., and Miller, M. S., "Curvature and Leading Edge Sweep Back Effects on Grid Fin Aerodynamic Characteristics," AIAA Paper 93-3480, Aug. 1993.

[6]Booth, P. F., and Washington, W. D., "Post Test Report for a Grid Fin Technology Wind Tunnel Test," U.S. Army Missile Command, System Simulation and Development Directorate, TR-RD-SS-89-6, Redstone Arsenal, AL, July 1989.

[7]Washington, W. D., and Booth, P. F., "Wind Tunnel Data Analysis for a Curved Grid Fin Concept," 16th Meeting, TTCP Technical Panel W-2, Eglin Air Force Base, FL, May 1990.

[8]Roskam, J., *Methods for Estimating Drag Polars for Subsonic Airplanes*, published by the Author, Lawrence, KS, 1971.

[9]Jorgensen, L. H., "Prediction of Static Aerodynamic Characteristics for Slender Bodies Alone and with Lifting Surfaces to Very High Angles of Attack," Ames Research Center, NASA TM X-73,123, Moffett Field, CA, July 1976.

[10]Landingham, G. M., Deep, R. A., and Brazzel, C. E., "Aerodynamic Data Base," U.S. Army Missile Command, System Simulation Directorate, Redstone Arsenal, AL, Oct. 1981.